Effective medium theory of thin-plate acoustic metamaterials

Pei Li, Shanshan Yao, and Xiaoming Zhou[a)]
Key Laboratory of Dynamics and Control of Flight Vehicle, Ministry of Education, and School of Aerospace Engineering, Beijing Institute of Technology, Beijing 100081, China

Guoliang Huang
Department of Systems Engineering, University of Arkansas at Little Rock, Little Rock, Arkansas 72204

Gengkai Hu
Key Laboratory of Dynamics and Control of Flight Vehicle, Ministry of Education, and School of Aerospace Engineering, Beijing Institute of Technology, Beijing 100081, China

(Received 27 June 2013; revised 4 December 2013; accepted 3 March 2014)

Effective dynamic properties of acoustic metamaterials made of multilayered flexible thin-plates with periodically attached mass-spring resonators are studied. By using the transfer matrix method, the thin-plate acoustic metamaterial under the plane wave incidence is characterized by a homogeneous effective medium with anisotropic mass density. An approximate analytic expression of effective mass density is derived for a single-layer metamaterial in the normally incident case, and it is shown that the effective mass density can follow either Lorentz or Drude medium models. For the obliquely incident case, it is found that effective mass density is dependent on the lateral wave number of incident waves. Such spatial dispersion comes from the coincidence effect between the incident acoustic wave and flexural wave in the thin plate, and it occurs at much lower frequencies than that for a uniform plate without resonators. Based on the observed spatial dispersion, an acoustic device made of thin-plate metamaterials is designed for frequency-controlled acoustic directive radiation in the low-frequency regime. © *2014 Acoustical Society of America.*
[http://dx.doi.org/10.1121/1.4868400]

PACS number(s): 43.40.Dx, 43.20.Tb, 43.20.Ks [ANN] Pages: 1844–1852

I. INTRODUCTION

Acoustic metamaterials (MMs) have been attracting increasing interest in recent years due to their anomalous physical properties[1] and potential applications to low-frequency noise isolation,[2,3] sub-diffraction-limited acoustic imaging,[4,5] acoustic cloaking,[6,7] etc. The early work on acoustic metamaterials is focused on bulk MMs (Refs. 1, 8, and 9) which typically consist of hard cores surrounded by soft coatings and embedded in a relatively rigid matrix. However, in practical applications, there is a strong demand for designing lightweight and thin-layer MMs for low-frequency sound isolation[10] and absorption.[11] Recently, a two-dimensional membrane-type MM was developed by placing mass-weighted membranes as solid inclusions in the air.[2] In addition to the lightweight nature, the membrane-type MMs can be characterized by an effectively homogeneous media with trivial effective shear resistance, thus making them more preferable for acoustic wave control.

In contrast to membrane-type MMs, thin-plate MMs use a mass-attached thin plate instead of a membrane. Therefore, more rich phenomena can be expected due to the bending resistance of the plate. Thin-plate structures are widely used due to their high static stiffness and stiffness-to-weight ratio. They are usually stiffened or corrugated in practical applications. Sound properties can be improved in mid or high frequencies, but not for low frequencies.[12] To circumvent this problem, a thin plate is more often incorporated with local resonant units, forming a thin-plate MM. Hsu and Wu,[13] and Xiao *et al.*[14] suggested a thin epoxy plate containing a periodic array of lead discs hemmed around by rubber. Wu *et al.*,[15] Pennec *et al.*,[16] and Oudich *et al.*[17] reported a thin plate deposited with a square lattice of cylindrical stubs. A microstructure design of anisotropic mass density is also investigated for an elastic metamaterial numerically and experimentally.[18] The low-frequency band gap[19,20] of Lamb modes can be obtained in these plate structures because the locally resonant mechanism is similar to that of bulk MMs. Although the correlation between the bandgap effect and structural parameters has been extensively studied, little research has focused on acoustic wave interaction with thin-plate MMs. Recently, Xiao *et al.*[21] presented an initial study of low-frequency sound insulation by metamaterial-based thin plates. In view of the application for low-frequency acoustic wave manipulation, the acoustic wave interaction with thin-plate MMs should be studied more thoroughly.

This work will study the low-frequency acoustic property of thin-plate MMs using an effective medium approach. In our analytic model, the locally resonant units are represented by mass-spring resonators that are attached to a thin plate. Then analytic solutions are derived for plane acoustic waves incident on thin-plate MMs at arbitrary angles, as will be presented in Sec. II. The transfer matrix method used for retrieving effective material parameters is introduced in Sec. III, and an approximate expression of effective mass

[a)]Author to whom correspondence should be addressed. Electronic mail: zhxming@bit.edu.cn

density is derived for a single-layer MM under normally incident cases. Section IV shows the results of effective dynamic properties of thin-plate MMs. It is found that negative effective mass can be achieved by either the mass-spring resonator or the resonant vibration of the thin plate. For oblique incident waves, thin-plate structures are modeled as MMs with anisotropic mass density, and effective mass is dependent on the lateral wave number of incident waves. Such spatial dispersion effects can be employed to realize frequency-controlled acoustic directive radiation, as will be demonstrated in Sec. V.

II. THEORETICAL FORMULATION

The studied model is shown in Fig. 1. It is composed of parallel-stacked thin plates with a separation d, and each plate is attached with mass-spring resonators with period L, where the weight of the mass is m_1 and the spring coefficient is k_1. A plane acoustic wave is incident on the plate structure with an incident angle θ. The background medium is the air with mass density ρ_0 and sound velocity c_0.

With the Kirchhoff plate theory, the bending wave equation of a single plate with resonators is written in terms of the transverse displacement u as[12]

$$D\frac{\partial^4 u}{\partial y^4}+\rho h\frac{\partial^2 u}{\partial t^2}-\sum_{n=-\infty}^{+\infty}F\delta(y-nL)-\rho_0\left(\frac{\partial\Phi_l}{\partial t}-\frac{\partial\Phi_r}{\partial t}\right)=0, \tag{1}$$

where the flexural stiffness of the plate is $D=Eh^3/(12(1-\nu^2))$ with Young's modulus E, Poisson's ratio ν, thickness h, and mass density ρ. The third term in Eq. (1) is contributed from the mass-spring resonators, and the concentrated force F is given by

$$F=k_1(u_{\text{mass}}-u), \tag{2}$$

where u_{mass} is the displacement of the attached mass. The fourth term is acoustic loading from the air with Φ_l and Φ_r representing, respectively, the velocity potentials at the left and right surfaces of the plate. The particle velocity v is related to the potential Φ by $v=-\nabla\Phi$.

In the time-harmonic case, the transverse displacement u_i of the ith plate can be expressed as a series of space harmonics, due to the periodic arrangement of mass-spring resonators[22]

$$u_i(y,t)=\sum_{n=-\infty}^{+\infty}A_n^i e^{-j\left(k_y+2n\pi/L\right)y}e^{j\omega t}, \tag{3}$$

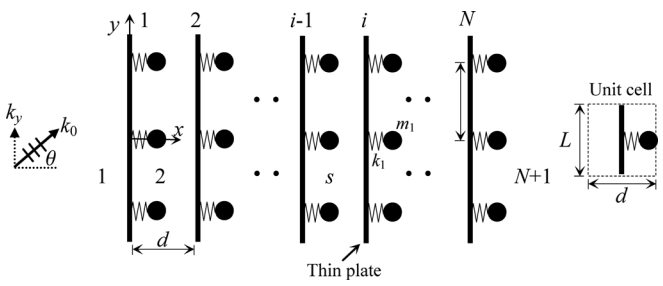

FIG. 1. The model of the thin-plate MM.

where A_n^i is the complex amplitude of the nth-order flexural mode for the ith plate. The equation of harmonic-wave motion of the resonator is given by $-m_1\omega^2 u_{\text{mass}}=k_1(u_i-u_{\text{mass}})$, thus the concentrated force in Eq. (2) is rewritten as

$$F_i=\frac{k_1\omega^2}{\omega_1^2-\omega^2}u_i(nL,t), \tag{4}$$

with $\omega_1=\sqrt{k_1/m_1}$.

Acoustic fields adjacent to the plates are also expected to be spatially periodic, then the velocity potentials in each region of the air are expressed as

$$\begin{aligned}\Phi_s=&\sum_{n=-\infty}^{+\infty}B_n^{s+}e^{-j\left[k_{xn}x+\left(k_y+2n\pi/L\right)y\right]}e^{j\omega t}\\&+\sum_{n=-\infty}^{+\infty}B_n^{s-}e^{-j\left[-k_{xn}x+\left(k_y+2n\pi/L\right)y\right]}e^{j\omega t},\\&s=1,2,\ldots,N+1,\end{aligned} \tag{5}$$

where $B_n^{1+}=1$ for incident waves, $B_n^{(N+1)-}=0$ due to nonreflecting waves in the transmission region ($s=N+1$), and B_n^{s+} and B_n^{s-} are unknown complex amplitudes of the forward and backward acoustic waves in the sth region of the air. k_{xn} is given by

$$k_{xn}=\begin{cases}\sqrt{k_0^2-\left(k_y+2n\pi/L\right)^2}, & k_0\geq k_y+2n\pi/L,\\ -j\sqrt{\left(k_y+2n\pi/L\right)^2-k_0^2}, & k_0<k_y+2n\pi/L,\end{cases} \tag{6}$$

with $k_0=\omega/c_0$.

At the boundaries between the plate and air, the continuous condition of the normal velocities results in

$$-\frac{\partial\Phi}{\partial x}=\frac{\partial u}{\partial t}. \tag{7}$$

By substitution of Eqs. (3) and (5) into Eq. (7), B_n^{s+} and B_n^{s-} can be expressed in terms of A_n^i by

$$B_n^{1-}=\begin{cases}\dfrac{-\omega A_n^1}{k_{xn}}+1 & (n=0),\\ \dfrac{-\omega A_n^1}{k_{xn}} & (n\neq 0),\end{cases} \tag{8a}$$

$$B_n^{s+}=\frac{e^{jk_{xn}(d+h)(-1+s)}\omega(e^{jdk_{xn}}A_n^{s-1}-A_n^s)}{(-1+e^{2jdk_{xn}})k_{xn}},\quad s=2,3,\ldots,N, \tag{8b}$$

$$B_n^{s-}=\frac{e^{-jk_{xn}(d(-2+s)+h(-1+s))}\omega(A_n^{s-1}-e^{jdk_{xn}}A_n^s)}{(-1+e^{2jdk_{xn}})k_{xn}},\quad s=2,3,\ldots,N, \tag{8c}$$

$$B_n^{(N+1)+}=\frac{\omega e^{jk_{xn}(Nh+(N-1)d)}A_n^N}{k_{xn}}. \tag{8d}$$

The unknown coefficients A_n^i can be solved from system equations that are derived by use of the virtual work

principle.[12,22] The virtual work principle states that the sum of the work contributed by all elements of the system must be equal to zero whenever the system undergoes the following virtual displacement:

$$\delta u^i = \delta A_n^i e^{-j(k_y+2n\pi/L)y} e^{j\omega t}. \tag{9}$$

The virtual work for the unit cell depicted in Fig. 1 is expressed as

$$\delta\Pi = \delta\Pi_P + \delta\Pi_F + \delta\Pi_R, \tag{10}$$

where $\delta\Pi_P$, $\delta\Pi_F$, and $\delta\Pi_R$ are the virtual work done by elastic and inertial forces of the plates, acoustic loading, and the concentrated force by the mass-spring resonator, respectively, and given by

$$\delta\Pi_P = \int_{-L/2}^{L/2} \left(D\frac{\partial^4 u_i}{\partial y^4} + \rho h \frac{\partial^2 u_i}{\partial t^2} \right) \delta\tilde{u}^i, \tag{11a}$$

$$\delta\Pi_F = \int_{-L/2}^{L/2} (-j\omega\rho_0(\Phi_i - \Phi_{i+1}))\delta\tilde{u}^i, \tag{11b}$$

$$\delta\Pi_R = -F\delta\tilde{u}^i, \tag{11c}$$

where $\delta\tilde{u}^i$ is the complex conjugate of the virtual displacement δu^i given in Eq. (9). According to the virtual work principle $\delta\Pi = 0$, the following system equations can be obtained:

$$\left(D\left(k_y + \frac{2n\pi}{L}\right)^4 - \rho h\omega^2 + \frac{2je^{2jdk_{xn}}\omega^2\rho_0}{(-1+e^{2jdk_{xn}})k_{xn}} \right) A_n^1 - \frac{1}{L}\frac{k_1\omega^2}{\omega_1^2-\omega^2} \sum_{q=-\infty}^{+\infty} A_q^1 - \frac{2je^{jdk_{xn}}\omega^2\rho_0}{(-1+e^{2jdk_{xn}})k_{xn}} A_n^2 = \begin{cases} 2j\omega\rho_0, & n=0 \\ 0, & n\neq 0 \end{cases} \tag{12a}$$

for the first plate ($i = 1$),

$$\left(D\left(k_y + \frac{2n\pi}{L}\right)^4 - \rho h\omega^2 + \frac{2j(1+e^{2jdk_{xn}})\omega^2\rho_0}{(-1+e^{2jdk_{xn}})k_{xn}} \right) A_n^i - \frac{1}{L}\frac{k_1\omega^2}{\omega_1^2-\omega^2} \sum_{q=-\infty}^{+\infty} A_q^i - \frac{2je^{jdk_{xn}}\omega^2\rho_0}{(-1+e^{2jdk_{xn}})k_{xn}} A_n^{i-1} - \frac{2je^{jdk_{xn}}\omega^2\rho_0}{(-1+e^{2jdk_{xn}})k_{xn}} A_n^{i+1} = 0 \tag{12b}$$

for the ith plate ($i = 2, 3, \ldots, N-1$), and

$$\left(D\left(k_y + \frac{2n\pi}{L}\right)^4 - \rho h\omega^2 + \frac{2je^{2jdk_{xn}}\omega^2\rho_0}{(-1+e^{2jdk_{xn}})k_{xn}} \right) A_n^N - \frac{1}{L}\frac{k_1\omega^2}{\omega_1^2-\omega^2} \sum_{q=-\infty}^{+\infty} A_q^N - \frac{2je^{jdk_{xn}}\omega^2\rho_0}{(-1+e^{2jdk_{xn}})k_{xn}} A_n^{N-1} = 0 \tag{12c}$$

for the Nth plate. The complex coefficients A_n^i can be computed from Eq. (12). The energy transmission and reflection coefficients of acoustic waves are calculated by

$$T = \sum_{n=-\infty}^{+\infty} |B_n^{(N+1)+}|^2 \mathrm{Re}(k_{xn})/k_{x0}, \tag{13a}$$

$$R = \sum_{n=-\infty}^{+\infty} |B_n^{1-}|^2 \mathrm{Re}(k_{xn})/k_{x0}. \tag{13b}$$

III. RETRIEVAL METHOD OF EFFECTIVE MATERIAL PARAMETER OF THIN-PLATE MMS

A. Transfer matrix method

In the general case, a multilayered thin-plate structure can be represented effectively by an acoustic fluid with anisotropic dynamic mass. The transfer matrix method, which has been widely used in the past to analyze and measure acoustical properties of porous materials,[23] will be employed here to evaluate effective medium properties of thin-plate MMs. For an effectively homogeneous medium with anisotropic mass density $\tilde{\boldsymbol{\rho}}_e = \mathrm{diag}[\rho_e, \rho_{\mathrm{ave}}]$ and thickness d_e, the transfer matrix $\mathbf{T}_e$ is defined by

$$\begin{bmatrix} p^A \\ v_x^A \end{bmatrix}_{x=0} = \mathbf{T}_e \begin{bmatrix} p^A \\ v_x^A \end{bmatrix}_{x=d_e}, \tag{14}$$

where p^A and v_x^A are the pressure and normal velocity, and

$$\mathbf{T}_e = \begin{bmatrix} \cos k_x d_e & (j\rho_e\omega/k_x)\sin k_x d_e \\ (jk_x/\rho_e\omega)\sin k_x d_e & \cos k_x d_e \end{bmatrix}, \tag{15}$$

with

$$\frac{k_x^2}{\rho_e} + \frac{k_y^2}{\rho_{\mathrm{ave}}} = \frac{\omega^2}{\kappa_e}, \tag{16}$$

where κ_e is effective bulk modulus. ρ_{ave} is the effective mass density for waves incident in the y direction, and follows the relation[24]

$$\frac{1}{\rho_{\mathrm{ave}}} = \frac{1}{d+h}\left(\frac{d}{\rho_0} + \frac{h}{\rho}\right). \tag{17}$$

The remaining unknown parameters ρ_e and κ_e can be retrieved by enforcing $\mathbf{T} = \mathbf{T}_e$, where $\mathbf{T}$ is the transfer matrix of the multilayered plates and can be computed according to analytic solutions derived in the above section. With the help of Eq. (15), it is obtained that

$$k_x = \pm\frac{1}{d_e}\cos^{-1} T_{11} + \frac{2\pi m}{d_e}, \quad m = 0, 1, 2, \ldots, \tag{18}$$

and

$$\rho_e = \frac{jk_x \sin k_x d_e}{\omega T_{21}}, \tag{19}$$

where $d_e = N(d+h)$. From Eq. (16), the effective bulk modulus is given by

$$\kappa_e = \frac{\omega^2}{k_x^2/\rho_e + k_y^2/\rho_{\mathrm{ave}}}. \tag{20}$$

B. Effective mass and modulus for a single-layer MM

To gain further insight into the relation between overall properties and structural parameters of the MM, analytic expression of effective mass density and modulus is expected for a single-layer MM in the long-wavelength limit. When the lowest two orders ($n = 0, \pm 1$) vibration modes are retained in this limit, Eq. (12) becomes in the normally incident case

$$\left(-\rho h\omega^2 + \frac{2j\omega^2\rho_0}{k_{x0}}\right)A_0 - \frac{1}{L}\frac{k_1\omega^2}{\omega_1^2-\omega^2}(A_0+A_1+A_{-1}) = 2j\omega\rho_0, \tag{21a}$$

$$\left(D\left(\frac{2\pi}{L}\right)^4 - \rho h\omega^2 + \frac{2j\omega^2\rho_0}{k_{x1}}\right)A_1 - \frac{1}{L}\frac{k_1\omega^2}{\omega_1^2-\omega^2}(A_0+A_1+A_{-1}) = 0, \tag{21b}$$

$$\left(D\left(\frac{2\pi}{L}\right)^4 - \rho h\omega^2 + \frac{2j\omega^2\rho_0}{k_{x(-1)}}\right)A_{-1} - \frac{1}{L}\frac{k_1\omega^2}{\omega_1^2-\omega^2}(A_0+A_1+A_{-1}) = 0, \tag{21c}$$

from which unknown coefficients A_0, A_1, A_{-1} can be determined. We then use the averaging field method to derive analytic expressions of effective mass density and effective modulus. For the unit cell of the single-layer MM, effective mass density is defined as the net force versus the total acceleration

$$\rho_{\text{eff}} = \frac{F_{\text{net}}}{a_p + a_{\text{air}}}, \tag{22}$$

where the net force F_{net} and accelerations of the plate a_p and air a_{air} are expressed as

$$F_{\text{net}} = j\rho_0\omega\left(\int_{-L/2}^{L/2}\Phi_1 dy - \int_{-L/2}^{L/2}\Phi_2 dy\right), \tag{23a}$$

$$a_p = h\int_{-L/2}^{L/2}\sum_{n=-1}^{n=1}A_n e^{-j(k_y+2n\pi/L)y}dy = -A_0 hL\omega^2, \tag{23b}$$

$$a_{\text{air}} = \int_{-L/2}^{L/2}\int_{-d/2}^{0}(-j\omega\nabla_x\Phi_1)dxdy + \int_{-L/2}^{L/2}\int_{0}^{d/2}(-j\omega\nabla_x\Phi_2)dxdy. \tag{23c}$$

In the long-wavelength case ($\lambda \gg L, d, h$), it is assumed that $e^{jk_{x0}d/2} \approx 1$ and $k_{x(\pm 1)} \approx -2j\pi/L$. Equation (22) is simplified as

$$\rho_e = \frac{2j\rho_0(1-A_0c_0)}{-A_0 h\omega(1+d/h)}. \tag{24}$$

Substituting A_0 that is solved from Eq. (21) into Eq. (24) results in

$$\rho_e = \frac{h}{d+h}\left(\rho + \frac{1}{hL}\frac{m_1\omega_1^2}{\omega_1^2 - \omega^2\left(1+\frac{2k_1L^3}{16D\pi^4 - L^4\rho h\omega^2}\right)}\right). \tag{25}$$

Effective modulus is defined as the total bulk stress versus the total bulk deformation

$$\kappa_e = \frac{\langle\sigma_b\rangle}{\langle\varepsilon_b\rangle}, \tag{26}$$

with

$$\langle\sigma_b\rangle = \int_{-L/2}^{L/2}\int_{-d/2}^{d/2}(\sigma_{ii}/3)dxdy, \tag{27a}$$

$$\langle\varepsilon_b\rangle = \int_{-L/2}^{L/2}\left[\left(-\frac{\nabla_x\Phi_1}{j\omega}\right)\Big|_{x=d/2} - \left(-\frac{\nabla_x\Phi_2}{j\omega}\right)\Big|_{x=-d/2}\right]dy. \tag{27b}$$

Assume $e^{jk_{x0}h} \approx 1$ in the limit $\lambda \gg L, d, h$, and neglect the bulk deformation in the thin plate. In the quasi-static case, Eq. (27) can be simplified as

$$\begin{aligned}\langle\sigma_b\rangle &= \int_{-L/2}^{L/2}\int_{-d/2}^{d/2} -p dxdy,\\ &= -j\omega\rho_0\left(\int_{-L/2}^{L/2}\int_{-d/2}^{0}\Phi_1 dxdy + \int_{-L/2}^{L/2}\int_{0}^{d/2}\Phi_2 dxdy\right),\\ &\approx -2jc_0L\rho_0\sin k_0 d/2,\end{aligned} \tag{28a}$$

$$\langle\varepsilon_b\rangle \approx -\frac{2jL\sin k_0 d/2}{c_0}. \tag{28b}$$

It can be deduced from Eqs. (26) and (28) that in the quasi-static case, the effective bulk modulus of the thin-plate metamaterial is close to that of the air $\kappa_e \approx \rho_0 c_0^2$.

IV. NUMERICAL RESULTS AND DISCUSSIONS

A. Effective mass density in normal incidence

Consider material parameters $E = 3.9\,\text{GPa}$, $\nu = 0.4$, and $\rho = 1400\,\text{kg/m}^3$ for the epoxy plate, and $h = 0.4\,\text{mm}$, $d = 4\,\text{mm}$. The mass density and sound velocity of the air are taken as $\rho_0 = 1.25\,\text{kg/m}^3$ and $c_0 = 343\,\text{m/s}$. For normally incident waves, Fig. 2 shows the real part of the effective mass density of single-layer MMs ($N = 1$) predicted by the transfer matrix method in three cases: (1) $L = 4\,\text{mm}$, (2) $L = 40\,\text{mm}$ with $k_1 = 10^4\text{N/m}$, $m_1 = 0.432\,\text{g}$, and (3) simply supported plates ($k_1, m_1 \to \infty$) with periodicity $L = 40\,\text{mm}$.

Shown in the first case of Fig. 2 is the result of relatively small periodicity $L = 4\,\text{mm}$. The resonant frequency of MMs, at which effective mass density approaches infinity, is 758 Hz, and is very close to that of mass-spring resonator $\omega_1/2\pi = 767\,\text{Hz}$. When further simplified for small values of

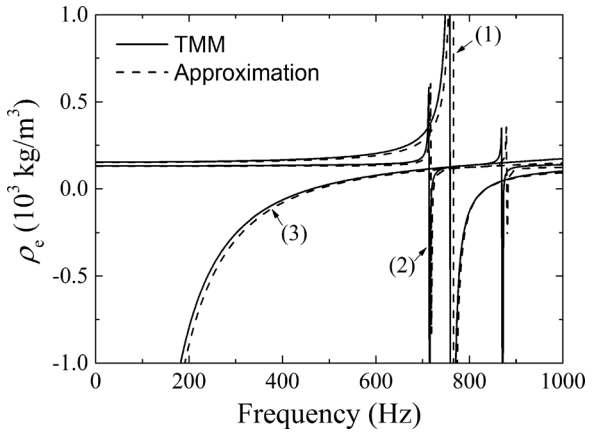

FIG. 2. Effective mass density ρ_e in normally incident case predicted by transfer matrix method (TMM) and approximate results in three cases: (1) $L = 4$ mm, (2) $L = 40$ mm with $k_1 = 10^4$ N/m, $m_1 = 0.432$ g, and (3) simply supported plates ($k_1, m_1 \to \infty$) with $L = 40$ mm.

L, Eq. (25) follows a typical expression of the Lorentz-medium model

$$\rho_{\text{eff}} = \frac{h}{d+h}\left(\rho + \frac{1}{hL}\frac{m_1\omega_1^2}{\omega_1^2 - \omega^2}\right). \tag{29}$$

The approximate result given by Eq. (29) is shown by the dashed line in Fig. 2 and agrees very well with that by TMM. Equation (29) is also the result of the rigid-plate case ($E \to \infty$), meaning that negative effective mass density can be realized due to the mass-spring resonance when the periodicity L is very small.

When L is increased to 40 mm, the negative effective mass can be obtained in two frequency bands, as shown in Fig. 2 for the second case. For comparison, the approximate result given by Eq. (25) is plotted by the dashed line and shows good agreement with that of TMM. To discover the physical mechanism whereby negative mass density arises in two separate bands, the resonant frequencies given by the TMM are shown in Fig. 3 for different periodicity L. For a pure plate of width L, the natural frequencies of first ($n = 1$) and second ($n = 2$) order symmetric modes are displayed in Fig. 3 for comparison, which are computed according to $\rho h\omega^2/D = (2n\pi/L)^4$. As a reference, the resonant frequency 767 Hz of the mass-spring resonator is also plotted. It can be seen that the resonant frequency of the MMs coincides with those of either the plate or the mass-spring resonator in the length scales of L far away from their crossover region. This means that, in addition to mass-spring resonance, the flexural vibration of the thin plate provides a new mechanism for negative effective mass density. A similar mechanism has also been reported in a flexible plate patterned periodically with heavy gratings.[25] The second case in Fig. 2 is taken near the crossover region belonging to the first-order flexural mode of the plate, where it is the hybrid vibration mode of the mass-attached plate that contributes to negative effective mass density. The second-order flexural mode appears at high L, which provides an addition band of negative mass in the frequency region of interest. Since the result (25) is derived under the first-order approximation, it shows a very good agreement with the first branch of the TMM results and parts of the second branch where the second-order flexural mode is not involved much.

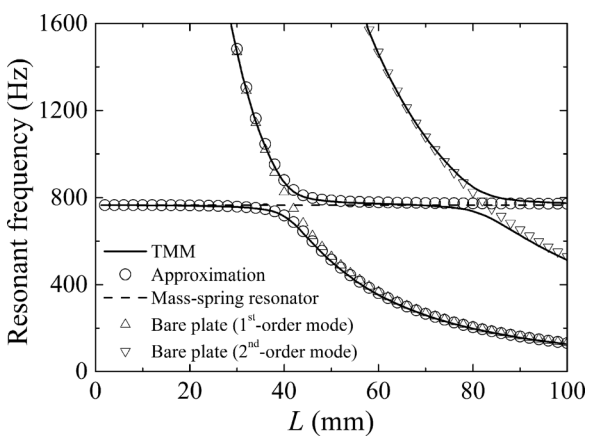

FIG. 3. Resonant frequencies of the MMs predicted by TMM and approximate results (25), the resonant frequency 767 Hz of mass-spring resonators, and natural frequencies of the first and second order flexural modes of a bare plate of the width L.

In the third case, the simply supported plate (k_1, $m_1 \to \infty$) is considered, and Eq. (25) is reduced to

$$\rho_e = \frac{h}{d+h}\left(\frac{3}{2}\rho - \frac{8D\pi^4}{hL^4\omega^2}\right). \tag{30}$$

Effective mass density given by Eq. (30) is shown in Fig. 2 by the dashed line, which coincides with that of the TMM. The results demonstrate that the thin-plate MM composed of simply supported plates follows the Drude-medium models with negative effective mass below the cut-off frequency 464 Hz. According to Eq. (30), the cut-off frequency is proportional to the plate rigidity D, consistent with the observation in a clamped plate.[26]

For the MMs composed of multilayered plates ($N \geq 2$), multiple scattering among plates may differentiate their effective properties from those of single-layer MMs. Taking the MM of the third case in Fig. 2 as an example, Fig. 4 shows the transmission amplitudes of normally incident waves for different numbers of plates ($N = 1, 2, \ldots, 6$). For all cases in Fig. 4, the first peak in transmission is due to near zero effective mass around the cut-off frequency 464 Hz. Since the cut-off frequency is mainly associated with the eigenfrequency of a single plate,[5] the frequency of the first transmission peak is invariant to the plate numbers. Multiple scattering prevails in the region beyond 464 Hz, where the effective mass density of the single layer is positive. As a result, thin-plate MMs behave as a one-dimensional periodic structure, and additional transmission peaks appear in the case of $N > 1$ due to the standing wave resonance in the periodic structure. So the effective medium description is only available in the region around and below the cut-off frequency, where multiple scattering effects can be negligible. Figure 5 shows the effective mass density of MMs with different numbers of layers. In the effective medium region, the effective mass density varies with very small fluctuations with the change of layer number.

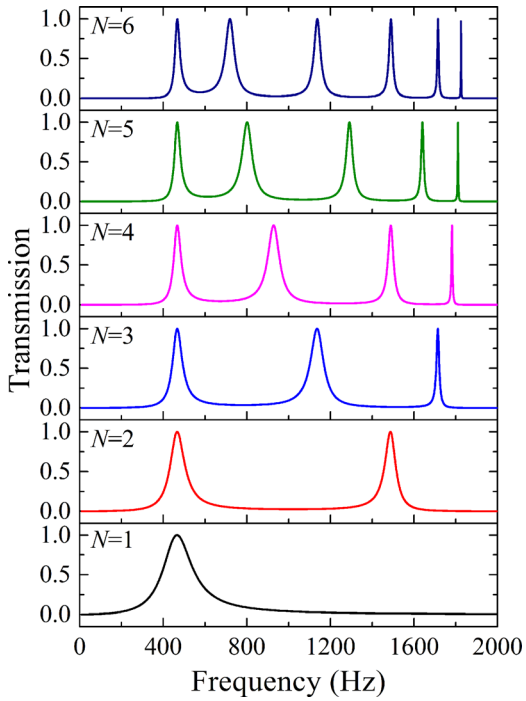

FIG. 4. (Color online) Transmission amplitudes of acoustic waves normally incident on MMs composed of a different number of plates ($N = 1, 2, \ldots, 6$).

B. Effective mass density in oblique incidence

For oblique incidence, the effective mass density of thin-plate MMs follows:

$$\tilde{\boldsymbol{\rho}}_e = \begin{bmatrix} \rho_e & 0 \\ 0 & \rho_{\text{ave}} \end{bmatrix},$$

where ρ_{ave} was given by Eq. (17) and ρ_e will be examined below. Consider the single-layer MM used in the example of Fig. 4 with two different plate thicknesses 0.4 and 1.5 mm. Figure 6(a) shows effective mass density ρ_e for three incident angles $\theta = 0, \pi/6, \pi/3$. In the case of $h = 0.4$ mm, effective mass density is almost invariant to the incident angle. When the plate thickness is increased to $h = 1.5$ mm, the dependence of ρ_e on the incident angle becomes noticeable. It is important to note for the latter case that effective

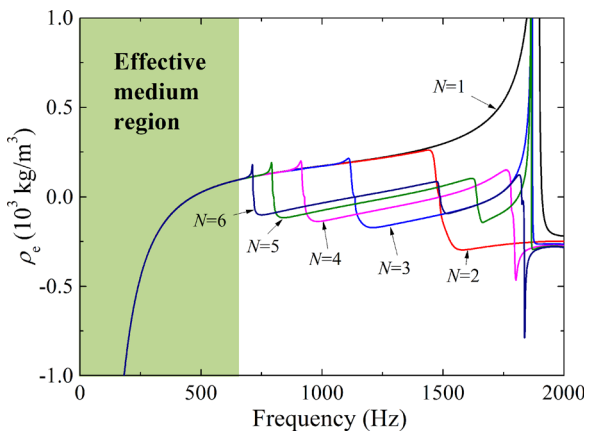

FIG. 5. (Color online) Effective mass density of MMs composed of different number (N) of plates versus the frequency.

mass density $\rho_e(\omega, k_y)$ will be written as a function of not only temporal frequency ω, but also the spatial one k_y. From the physical point of view, k_y-dependent material parameters can be attributed to the spatial dispersion in structured materials, and are very likely to appear when the periodicity of the unit cell is in the order of the wavelength.[27] For thin-plate MMs, the factor that dominates the spatial dispersion can be explored by examining the coincidence effect between acoustic wave and flexural wave in the plate structure. In the case of uniformly homogeneous plates, the coincidence phenomenon takes place when the lateral wavenumber k_y of the incident acoustic wave is coincident with the flexural wavenumber of the plate, and a maximum of wave transmission can be observed as a result. For the structured MMs, transmission peaks can be clearly observed at near-zero-mass frequencies, as shown in Fig. 6(b). To verify if the coincidence condition is exact for the structured MMs, the flexural wavenumber $k_b(\omega)$ of the structured plate is plotted in Fig. 7 against frequency. The computation method for $k_b(\omega)$ is provided in the Appendix. The lateral wavenumber k_y of the incident wave versus the coincidence frequency, which is designated as the peak transmission frequency, is shown in Fig. 7 for comparison, and excellent agreement can be observed between both results.

The physical interpretation of the spatial dispersion of the thin-plate MMs is thus given by the fact that there is no unique frequency for different flexural wavenumbers of the structured plate. Therefore acoustic responses and associated effective medium properties of the MMs are relevant to the incident angle due to the coincidence effect between acoustic wave and the flexural vibration of the plate. As can be seen in Fig. 7, the spatial dispersion is very weak in the case of $h = 0.4$ mm because the frequency 464 Hz remains almost unchanged with respect to the flexural wavenumber. This is often the case when the acoustic wavelength is much greater than the periodicity, for example, $\lambda_0 = 18.4L$ in this case. In the case of $h = 1.5$ mm, it is evident that the spatial dispersion becomes noticeable due to the non-zero slope for the dispersion curve. The frequency is 1753 Hz at $k_b = 0$, and the corresponding wavelength satisfies $\lambda_0 = 4.9L$. The above results may conclude that the spatial dispersion of the MMs appears in a relatively small λ_0/L and its presence can be explained by the dispersion effect of the flexural vibration of the structured plate.

For comparison, Fig. 8 shows results similar to those in Fig. 7 but for the uniform plate without resonators, where the dispersion relation of the uniform plate plotted by the solid line is given by $k_b^4 = \omega^2 \rho h / D$. These results means that the spatial dispersion is always present in a uniform plate, and therefore the peak transmission frequency depends on the incident angle. However, there exists the lowest coincidence frequency f_{low} for a uniform plate, which is predicted by[28]

$$f_{\text{low}} = \frac{c_0^2}{2\pi} \sqrt{\frac{\rho h}{D}}. \tag{31}$$

As seen in Fig. 8, the lowest coincidence frequencies for both cases $h = 0.4$ mm and $h = 1.5$ mm are much higher than

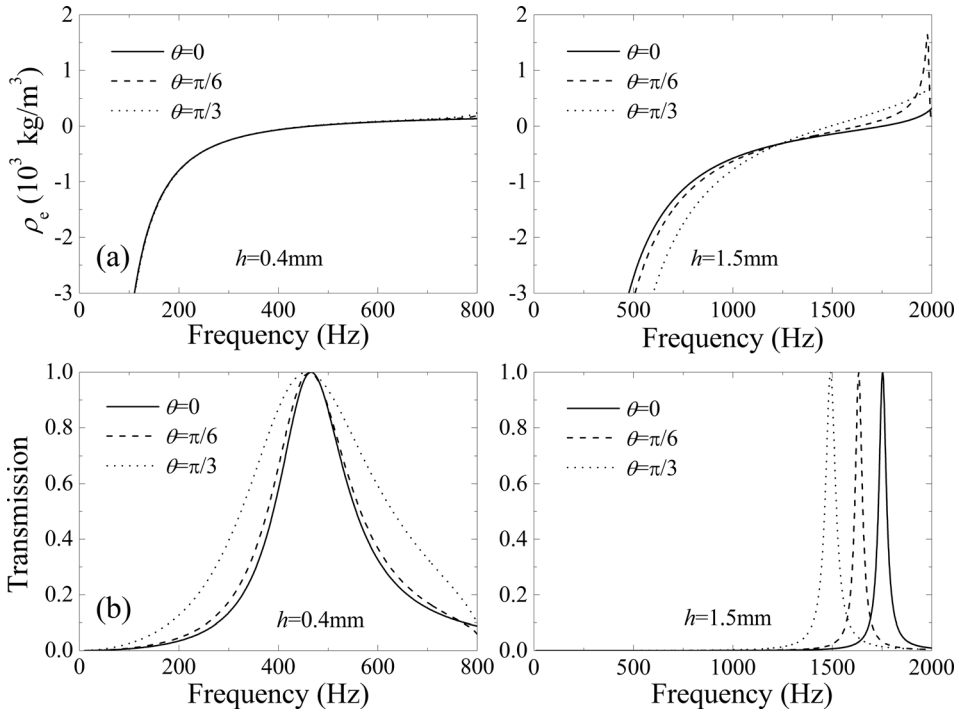

FIG. 6. (a) Transmission amplitudes and (b) effective mass density ρ_e of thin-plate MMs with the plate thicknesses 0.4 and 1.5 mm for three different incident angles $\theta = 0,\ \pi/6,\ \pi/3$.

those observed for the structured plate with resonators (Fig. 7). So the role played by the presence of the attached resonators is that the resonance and coincidence frequencies of the structured plate will be drastically reduced in comparison to the uniform plate. This means that a structured plate with resonators is superior to a uniform plate for application to low-frequency wave manipulation.

V. APPLICATION TO ACOUSTIC DIRECTIVE RADIATION

Acoustic MMs composed of simply supported plates ($k_1, m_1 \to \infty$) can be used to block low-frequency noises in the frequency range of negative effective mass density. For noise-isolation applications, the absence of the spatial dispersion of MMs may be preferred since there is a unique cut-off frequency for incoming waves with arbitrary direction of incidence. This section will present the MM's application to frequency-controlled directive radiation, whose underlying mechanism relies on the spatial dispersion effect. The basic principle of this application can be understood from the results of the case $h = 1.5$ mm in Fig. 6(b). For a specific frequency, wave transmission reaches the maximum at the coincidence angle, where effective mass density is near zero. The transmission amplitude will be suppressed in angles different than the coincidence one due to the spatial dispersion of the MMs. As a result, a narrow band of high transmission will be formed in the angular spectrum, which can be used for directive radiation. More importantly, the coincidence angle will be shifted when the frequency is changed. This means that the radiation angle can be tuned by modifying only the operating frequency without a change to the MM structure.

The device for acoustic directive radiation is constructed by placing a sound source behind a MM, forming a radiation pattern in the front region of the MM. For numerical verification, the proposed MM is made of epoxy plates possessing the

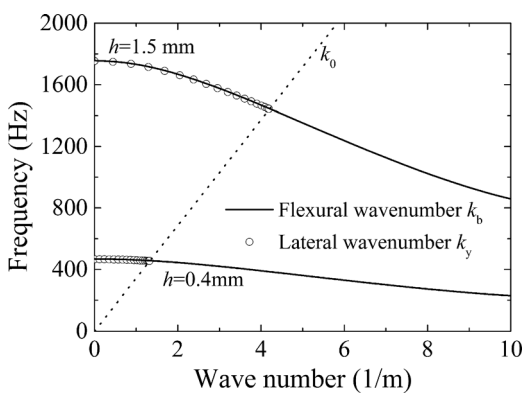

FIG. 7. The dispersion curve for flexural waves (k_b) propagating in the plate with resonators (solid line) and the lateral wavenumber k_y of the incident wave versus the peak transmission frequency (hollow circle).

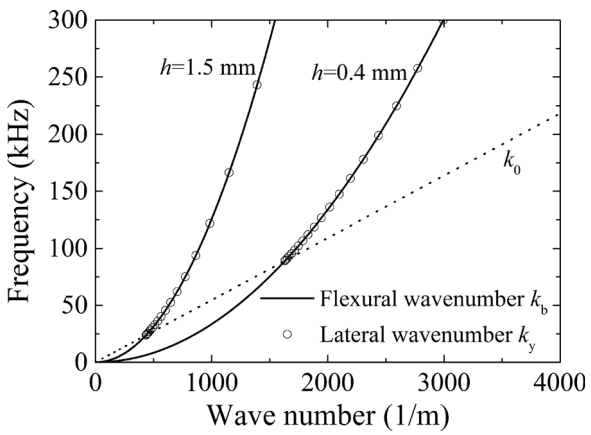

FIG. 8. The results similar to those in Fig. 7, but for the uniform plate without resonators.

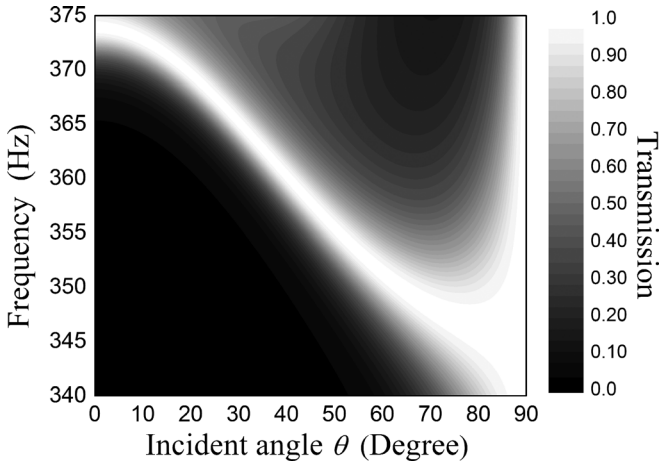

FIG. 9. Transmission amplitudes of acoustic waves incident on a thin-plate MM with different frequencies and incident angles.

following parameters: $L = 100\,\text{mm}$, $h = 2\,\text{mm}$, $d = 20\,\text{mm}$, and $N = 6$. Figure 9 shows wave transmission amplitudes for different frequency and incident angle, which are computed according to Eq. (13a). For incident angles close to $\theta = 90°$, the effective medium property of the MM is close to that of the air due to the small thickness-to-distance ratio h/d. As a consequence, wave transmission is enhanced in the vicinity of incident angle $\theta = 90°$. Apart from this angular region, a narrow band of high transmission can be clearly observed.

To evaluate the directive radiation by the MM device, numerical simulations were conducted by use of COMSOL MULTIPHYSICS. The distance between the sound source and the backside of the MM is 10 mm. Figure 10 shows by the solid line the simulation results of the radiation pattern in the front region of the device at four different frequencies: 373, 370, 365, and 360 Hz. The radiation pattern is depicted by the normalized pressure intensity defined as $|P_{\text{far}}|^2/|P_0|^2$, where P_{far} and P_0 are far field pressures in the presence and absence of the MM, respectively. Notice that the radiation pattern in the angular spectrum ranging from $-90°$ to $0°$ has been omitted due to the symmetry. For a comparison, transmission amplitudes given by the analytic results (13a) are plotted by the dashed line, and are in good agreement with the simulation results. The result clearly demonstrates that the thin-plate MM is capable of directive radiation with the radiation angle varied for different frequency. Note that the directivity can be enhanced when transmission peaks in both frequency and angular spectra are sharpened by increasing the layer number of the MMs.

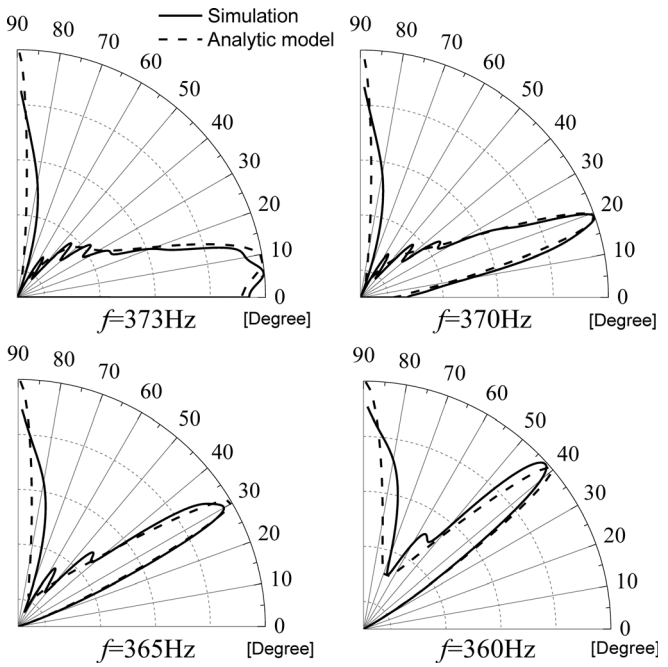

FIG. 10. Simulation and analytic results of radiation patterns in the front region of the metamaterial behind which an acoustic source operating at four frequencies: 373, 370, 365, and 360 Hz is placed with the distance 10 mm.

VI. CONCLUSIONS

Effective dynamic properties of multilayered thin plates with attached mass-spring resonators are examined based on analytic solutions for plane acoustic waves incident on the plate structures. For normal incidence, negative effective mass density can be realized by the resonance of either the mass-spring resonator or the plate matrix. It is found that Lorentz or Drude medium models for effective mass density can be easily realized by the structured plates. In the obliquely incident case, spatial dispersion has been observed in thin-plate MMs, and effective mass density is dependent on the incident angle as a result. As an application of this spatial dispersion, the thin-plate MMs are designed for directive radiation, and the radiation direction can be controlled by varying the operating frequency without changing the MM structure. Their potential application to underwater sonar detection is anticipated.

ACKNOWLEDGMENTS

This work was supported by the National Natural Science Foundation of China (Grant Nos. 10832002, 11172038, 11072031, 11302028, and 11221202), the National Basic Research Program of China (Grant No. 2011CB610302), and the Program for New Century Excellent Talents in University.

APPENDIX: DISPERSION RELATION FOR FLEXURAL WAVE IN THE THIN-PLATE STRUCTURE

Figure 11 shows one layer of the thin-plate MM depicted in Fig. 1. The method for computing the dispersion curves for flexural vibration of the thin plate will be presented below. In the time-harmonic case, the flexural wave equation of the thin plate follows:[20]

$$\frac{\partial^2}{\partial x^2}\left(D\frac{\partial^2 u}{\partial x^2}\right) - \rho h\omega^2 u = 0, \tag{A1}$$

where the transverse displacement of the plate is $u(x,t) = U(x)e^{j\omega t}$. The general solution $U(x)$ of Eq. (A1) can be expressed as

$$U(x) = c^1\cos(\alpha x) + c^2\sin(\alpha x) + c^3\cosh(\alpha x) + c^4\sinh(\alpha x), \tag{A2}$$

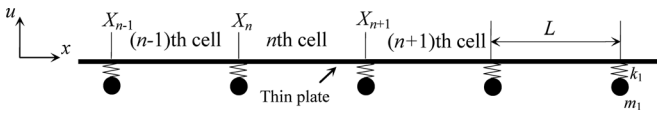

FIG. 11. A thin plate attached periodically with mass-spring resonators.

with $\alpha = \sqrt[4]{\rho h\omega^2/D}$. With the help of Eq. (A2), the displacement for the nth unit cell is written as

$$U_n(x'_n,t) = c_n^1\cos(\alpha x'_n) + c_n^2\sin(\alpha x'_n) + c_n^3\cosh(\alpha x'_n) + c_n^4\sinh(\alpha x'_n), \tag{A3}$$

with $x'_n = x - X_n$.

At the boundary $x = X_{n+1}$, the continuous conditions of the transverse displacement, slope, bending moment, and shear force are written by the following relations:

$$U_{n+1}(0) = U_n(L), \tag{A4a}$$

$$U'_{n+1}(0) = U'_n(L), \tag{A4b}$$

$$U''_{n+1}(0) = U''_n(L), \tag{A4c}$$

$$DU'''_{n+1}(0) - \frac{k_1\omega^2}{\omega_1^2-\omega^2}U_{n+1}(0) = DU'''_n(L). \tag{A4d}$$

Equation (A4) is written in the matrix form as

$$\mathbf{K}\boldsymbol{\Psi}_{n+1} = \mathbf{H}\boldsymbol{\Psi}_n, \tag{A5}$$

where $\boldsymbol{\psi}_n = \left[C_n^1,\ C_n^2, C_n^3, C_n^4\right]^T$ and $F = -k_1\omega^2/(D\alpha^3(\omega_1^2-\omega^2))$,

$$\mathbf{K} = \begin{bmatrix} 1 & 0 & 1 & 0 \\ 0 & 1 & 0 & 1 \\ -1 & 0 & 1 & 0 \\ F & -1 & F & 1 \end{bmatrix}, \tag{A6}$$

$$\mathbf{H} = \begin{bmatrix} \cos(\alpha L) & \sin(\alpha L) & \cosh(\alpha L) & \sinh(\alpha L) \\ -\sin(\alpha L) & \cos(\alpha L) & \sinh(\alpha L) & \cosh(\alpha L) \\ -\cos(\alpha L) & -\sin(\alpha L) & \cosh(\alpha L) & \sinh(\alpha L) \\ \sin(\alpha L) & -\cos(\alpha L) & \sinh(\alpha L) & \cosh(\alpha L) \end{bmatrix}. \tag{A7}$$

By use of the periodic condition for the unit cell, it is obtained that

$$\boldsymbol{\Psi}_{n+1} = e^{jqL}\boldsymbol{\Psi}_n, \tag{A8}$$

where q is the Bloch wave number. Combining Eqs. (A5) and (A8), the dispersion equation

$$|\mathbf{K}^{-1}\mathbf{H} - e^{jqL}\mathbf{I}| = 0 \tag{A9}$$

is obtained, where $\mathbf{I}$ is the fourth-order identity tensor.

[1]Z. Liu, X. Zhang, Y. Mao, Y. Y. Zhu, Z. Yang, C. T. Chan, and P. Sheng, "Locally resonant sonic materials," Science **289**(5485), 1734–1736 (2000).
[2]Z. Yang, J. Mei, M. Yang, N. Chan, and P. Sheng, "Membrane-type acoustic metamaterial with negative dynamic mass," Phys. Rev. Lett. **101**(20), 204301 (2008).
[3]C. J. Naify, C.-M. Chang, G. McKnight, and S. Nutt, "Transmission loss and dynamic response of membrane-type locally resonant acoustic metamaterials," J. Appl. Phys. **108**(11), 114905 (2010).
[4]J. Zhu, J. Christensen, J. Jung, L. Martin-Moreno, X. Yin, L. Fok, X. Zhang, and F. J. Garcia-Vidal, "A holey-structured metamaterial for acoustic deep-subwavelength imaging," Nat. Phys. **7**(1), 52–55 (2011).
[5]X. Zhou and G. Hu, "Superlensing effect of an anisotropic metamaterial slab with near-zero dynamic mass," Appl. Phys. Lett. **98**(26), 263510 (2011).
[6]S. Zhang, C. Xia, and N. Fang, "Broadband acoustic cloak for ultrasound waves," Phys. Rev. Lett. **106**(2), 024301 (2011).
[7]B.-I. Popa, L. Zigoneanu, and S. A. Cummer, "Experimental acoustic ground cloak in air," Phys. Rev. Lett. **106**(25), 253901 (2011).
[8]Z. Liu, C. Chan, and P. Sheng, "Analytic model of phononic crystals with local resonances," Phys. Rev. B **71**(1), 014103 (2005).
[9]X. Zhou and G. Hu, "Analytic model of elastic metamaterials with local resonances," Phys. Rev. B **79**(19), 195109 (2009).
[10]Z. Yang, H. M. Dai, N. H. Chan, G. C. Ma, and P. Sheng, "Acoustic metamaterial panels for sound attenuation in the 50–1000 Hz regime," Appl. Phys. Lett. **96**(4), 041906 (2010).
[11]J. Mei, G. Ma, M. Yang, Z. Yang, W. Wen, and P. Sheng, "Dark acoustic metamaterials as super absorbers for low-frequency sound," Nat. Commun. **3**, 756 (2012).
[12]J. Wang, T. J. Lu, J. Woodhouse, R. S. Langley, and J. Evans, "Sound transmission through lightweight double-leaf partitions: theoretical modelling," J. Sound Vib. **286**(4–5), 817–847 (2005).
[13]J.-C. Hsu and T.-T. Wu, "Lamb waves in binary locally resonant phononic plates with two-dimensional lattices," Appl. Phys. Lett. **90**(20), 201904 (2007).
[14]W. Xiao, G. W. Zeng, and Y. S. Cheng, "Flexural vibration band gaps in a thin plate containing a periodic array of hemmed discs," Appl. Acoust. **69**(3), 255–261 (2008).
[15]T.-T. Wu, Z.-G. Huang, T.-C. Tsai, and T.-C. Wu, "Evidence of complete band gap and resonances in a plate with periodic stubbed surface," Appl. Phys. Lett. **93**(11), 111902 (2008).
[16]Y. Pennec, B. Djafari-Rouhani, H. Larabi, J. O. Vasseur, and A. C. Hladky-Hennion, "Low-frequency gaps in a phononic crystal constituted of cylindrical dots deposited on a thin homogeneous plate," Phys. Rev. B **78**(10), 104105 (2008).
[17]M. Oudich, Y. Li, B. M. Assouar, and Z. Hou, "A sonic band gap based on the locally resonant phononic plates with stubs," New J. Phys. **12**(8), 083049 (2010).
[18]R. Zhu, X. N. Liu, G. L. Huang, H. H. Huang, and C. T. Sun, "Microstructural design and experimental validation of elastic metamaterial plates with anisotropic mass density," Phys. Rev. B **86**(14), 144307 (2012).
[19]Z.-J. Yao, G.-L. Yu, Y.-S. Wang, and Z.-F. Shi, "Propagation of bending waves in phononic crystal thin plates with a point defect," Int. J. Solids Struct. **46**(13), 2571–2576 (2009).
[20]Y. Liu, D. Yu, L. Li, H. Zhao, J. Wen, and X. Wen, "Design guidelines for flexural wave attenuation of slender beams with local resonators," Phys. Lett. A **362**(5–6), 344–347 (2007).
[21]Y. Xiao, J. H. Wen, and X. S. Wen, "Sound transmission loss of metamaterial-based thin plates with multiple subwavelength arrays of attached resonators," J. Sound Vib. **331**(25), 5408–5423 (2012).
[22]D. J. Mead and K. K. Pujara, "Space-harmonic analysis of periodically supported beams: Response to convected random loading," J. Sound Vib. **14**(4), 525–541 (1971).
[23]B. H. Song and J. S. Bolton, "A transfer-matrix approach for estimating the characteristic impedance and wave numbers of limp and rigid porous materials," J. Acoust. Soc. Am. **107**(3), 1131–1152 (2000).
[24]D. Torrent and J. Sánchez-Dehesa, "Anisotropic mass density by radially periodic fluid structures," Phys. Rev. Lett. **105**(17), 174301 (2010).
[25]Z. He, C. Qiu, L. Cheng, M. Xiao, K. Deng, and Z. Liu, "Negative-dynamic-mass response without localized resonance," Europhys. Lett. **91**(5), 54004 (2010).
[26]S. S. Yao, X. M. Zhou, and G. K. Hu, "Investigation of the negative-mass behaviors occurring below a cut-off frequency," New J. Phys. **12**, 103025 (2010).
[27]C. Menzel, C. Rockstuhl, T. Paul, F. Lederer, and T. Pertsch, "Retrieving effective parameters for metamaterials at oblique incidence," Phys. Rev. B **77**(19), 195328 (2008).
[28]M. J. Crocker, *Handbook of Noise and Vibration Control* (Wiley, New York, 2007), Chap. 6, pp. 79–100.